Article

Cell

Long-Lived Binding of Sox2 to DNA Predicts Cell Fate in the Four-Cell Mouse Embryo

Graphical Abstract

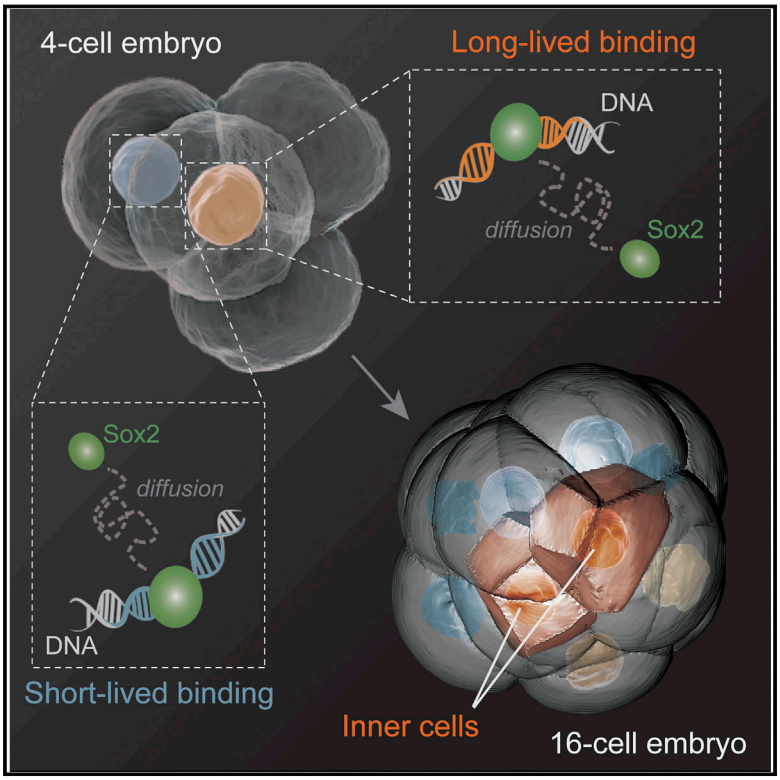

Authors

Melanie D. White, Juan F. Angiolini, Yanina D. Alvarez, ..., Stephanie Bissiere, Valeria Levi, Nicolas Plachta

Correspondence

vlevi12@gmail.com (V.L.), plachtan@imcb.a-star.edu.sg (N.P.)

In Brief

Quantification of the dynamics of Sox2-DNA binding in single cells of live mouse embryos shows that its heterogeneities in four-cell blastomeres are regulated by histone methylation and predict a bias in the contribution of cells to the inner mass.

Highlights

- Transcription factors display temporally distinct DNA binding in live mouse embryos
- Sox2-DNA binding is heterogeneous between four-cell blastomeres within the embryo
- Histone 3 arginine 26 methylation regulates Sox2-DNA binding
- More Sox2 engaged in long-lived DNA binding predicts inner cell allocation

White et al., 2016, Cell *165*, 75–87
March 24, 2016
http://dx.doi.org/10.1016/j.cell.2016.02.032

CellPress

Cell

Long-Lived Binding of Sox2 to DNA Predicts Cell Fate in the Four-Cell Mouse Embryo

Melanie D. White,[1,3] Juan F. Angiolini,[2,3] Yanina D. Alvarez,[2,3] Gurpreet Kaur,[1,3] Ziqing W. Zhao,[1] Esteban Mocskos,[2] Luciana Bruno,[2] Stephanie Bissiere,[1] Valeria Levi,[2,*] and Nicolas Plachta[1,*]
[1]Institute of Molecular and Cell Biology, A*STAR, 61 Biopolis Drive, Singapore 138673, Singapore
[2]Facultad de Ciencias Exactas y Naturales, Universidad de Buenos Aires, CONICET, Buenos Aires C1428EHA, Argentina
[3]Co-first author
*Correspondence: vlevi12@gmail.com (V.L.), plachtan@imcb.a-star.edu.sg (N.P.)
http://dx.doi.org/10.1016/j.cell.2016.02.032

SUMMARY

Transcription factor (TF) binding to DNA is fundamental for gene regulation. However, it remains unknown how the dynamics of TF-DNA interactions change during cell-fate determination in vivo. Here, we use photo-activatable FCS to quantify TF-DNA binding in single cells of developing mouse embryos. In blastocysts, the TFs Oct4 and Sox2, which control pluripotency, bind DNA more stably in pluripotent than in extraembryonic cells. By contrast, in the four-cell embryo, Sox2 engages in more long-lived interactions than does Oct4. Sox2 long-lived binding varies between blastomeres and is regulated by H3R26 methylation. Live-cell tracking demonstrates that those blastomeres with more long-lived binding contribute more pluripotent progeny, and reducing H3R26 methylation decreases long-lived binding, Sox2 target expression, and pluripotent cell numbers. Therefore, Sox2-DNA binding predicts mammalian cell fate as early as the four-cell stage. More generally, we reveal the dynamic repartitioning of TFs between DNA sites driven by physiological epigenetic changes.

INTRODUCTION

Transcription factors (TFs) regulate gene expression and cell fate during development (Ben-Tabou de-Leon and Davidson, 2007). In the early mammalian embryo, the TFs Oct4 and Sox2 are required in the pluripotent cell lineage (Avilion et al., 2003; Boyer et al., 2006; Nichols et al., 1998; Rosner et al., 1990; Schöler et al., 1990). However, most cells express these proteins homogenously during early development (Avilion et al., 2003; Plachta et al., 2011), and thus, it is perplexing why only some cells acquire a pluripotent fate. Recent studies propose that the function of various transcriptional regulators depends not only on expression levels but also on dynamic changes in intracellular distribution that could ultimately affect DNA binding (Ashall et al., 2009; Cai et al., 2008; Cohen-Saidon et al., 2009; Purvis et al., 2012). Yet the spatio-temporal dynamics of TF-DNA binding in single cells in vivo remain poorly understood.

Furthermore, it remains debated precisely when and how the blastomeres of the mammalian embryo adopt their first lineage fates (Burton and Torres-Padilla, 2014; Rossant and Tam, 2009; Zernicka-Goetz et al., 2009). Unlike in some non-mammalian species, identifying heterogeneities predicting cell fate in the early mouse and human embryo has proven challenging. The morphological uniformity and lack of evidence for uneven distribution of fate determinants in mouse blastomeres led to a primarily stochastic view of fate determination (Rossant, 1976; Tarkowski and Wróblewska, 1967). Studies have supported this view with analyses of TF expression levels in fixed embryos (Dietrich and Hiiragi, 2007), time-lapse imaging with differential interference contrast optics, or fluorescently labeled cell nuclei (Kurotaki et al., 2007; Louvet-Vallée et al., 2005; Motosugi et al., 2005). These investigations concluded that the separation of pluripotent and extraembryonic fates is unpredictable until the 16- to 32-cell stage. However, analysis of fixed specimens cannot establish direct cell-lineage relationships, and tracking cell nuclei alone is inaccurate because nuclear spatial coordinates cannot be translated into position and morphology of the entire cell.

By contrast, others propose that mammalian cell fates are predictable as early as the 2- or 4-cell stage (Gardner, 2001; Piotrowska-Nitsche et al., 2005; Shi et al., 2015). The identification of heterogeneities in H3 arginine methylation levels between four-cell blastomeres of the mouse embryo (Torres-Padilla et al., 2007) provided an entry point to examine the role of epigenetic variability in cell-fate decisions. Overexpression of the H3 arginine-methylating enzyme Carm1 biased blastomeres toward the pluripotent inner mass. Therefore, it was suggested that higher H3 arginine methylation levels promote a more open chromatin state, which may facilitate the acquisition of pluripotent fates. However, since measuring histone methylation requires embryo fixation, it is yet to be demonstrated how H3 arginine methylation levels might regulate pluripotency and whether different methylation patterns give rise to distinct fates in intact developing embryos. Since histone modifications control DNA accessibility, they may regulate TF-DNA binding dynamics. However, the lack of tools to analyze TF-DNA binding at the single-cell level in vivo has impeded these investigations.

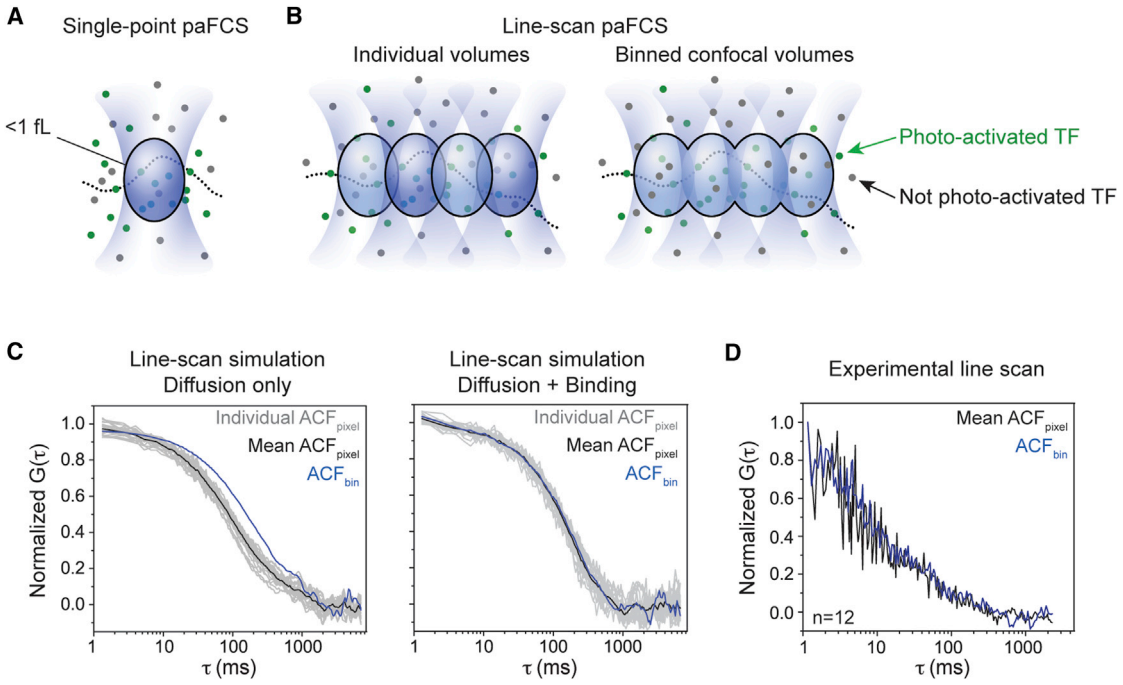

Figure 1. Line Scan paFCS Distinguishes TF Diffusion from Binding

(A) In paFCS, a selected number of TFs are photo-activated with 820 nm light. Fluorescence intensity fluctuations are measured within a confocal volume.

(B) paFCS and line scanning enables measurements within adjacent individual (left) or binned (right) confocal volumes. Dotted lines trace diffusion trajectories.

(C) Simulations of line scan experiments for individual and binned volumes. For molecules exhibiting diffusion only (left), the ACF curve for the binned volumes (ACF_{bin}) shifts to higher τ values relative to the curves obtained at each volume (ACF_{pixel}). When binding is present (right), the ACF curves are indistinguishable.

(D) Oct4-paGFP experiments in mouse ESCs. The mean ACF_{pixel} and ACF_{bin} are largely indistinguishable, indicating that fluctuations in the 1- to 300-ms window result from binding, and not diffusion. Diffusion events are not observed in the line scan ACFs since the line sampling time is longer than the characteristic diffusion time. n, number of cells.

See also Figure S1.

Traditionally, TF-DNA binding has been studied with biochemical methods in cell homogenates. As such approaches mask cell-to-cell variability, they prompted an interpretation that TFs form largely stable complexes with DNA (Perlmann et al., 1990). Recent advances in live-cell imaging reveal a more dynamic picture (Gorman and Greene, 2008; Hager et al., 2009; Halford and Marko, 2004; Mueller et al., 2013). Single-molecule tracking (SMT) of fluorescently labeled TFs in cultured cells demonstrated that TF-DNA interactions cannot be interpreted as a homogeneous population of molecules binding uniformly to DNA. Instead, TFs display temporally distinct binding interactions ranging from milliseconds to seconds (Chen et al., 2014; Gebhardt et al., 2013; Normanno et al., 2012). Shorter-lived binding is proposed to occur at non-consensus "off-target" sites (Chen et al., 2014; Gorman and Greene, 2008; Mueller et al., 2013; von Hippel and Berg, 1989). These transient events, involving 1D sliding of the TFs along DNA, interspersed with hopping and intersegmental transfer, allow TFs to scan the genome more efficiently than via 3D diffusion alone. Conversely, longer-lived interactions are proposed to occur at DNA sites for which the TF has higher affinity and are assumed to represent specific binding events that lead to transcription (Hager et al., 2009; Mueller et al., 2013).

Despite such progress, these ideas have not been tested in the context of cell-fate determination and mammalian development. It is unknown how transient TF-DNA binding events are in vivo, how TFs repartition between binding sites, and how TF-DNA binding dynamics may be modulated by epigenetic changes controlling cell fate. Here, we address these questions in developing mouse embryos by probing the DNA-binding dynamics of Oct4 and Sox2.

RESULTS

Line Scan paFCS Discriminates Temporally Distinct TF-DNA Binding Events

Fluorescence correlation spectroscopy (FCS) measures fluctuations in fluorescence intensity when molecules move through a small observation volume (Digman and Gratton, 2011), and an autocorrelation analysis of the traces reveals the mobility of the molecules (Figure 1A). To obtain optimal autocorrelation data, we recently fused TFs to photo-activatable GFP (paGFP), enabling us to fine-tune the number of fluorescent molecules. We found that one fraction of Oct4 and Sox2 molecules displays rapid Brownian diffusion, whereas the other fraction displays slower and anomalous diffusion (Kaur et al., 2013).

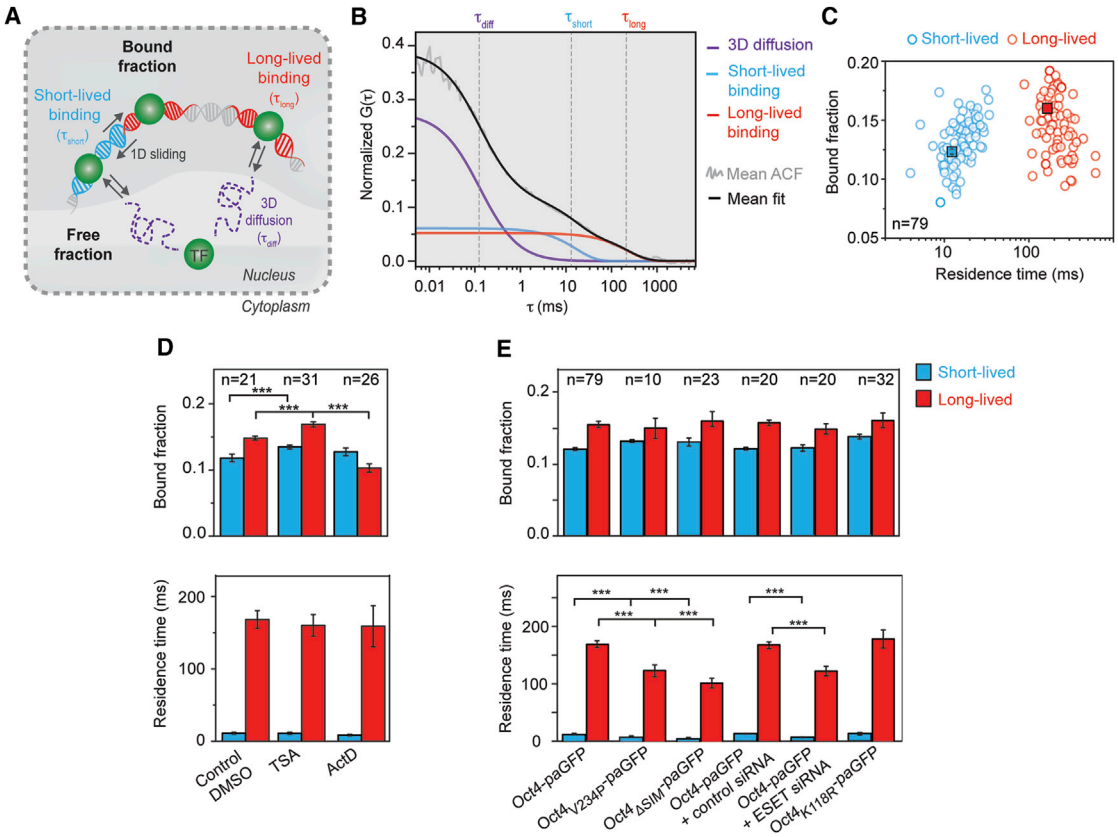

Figure 2. TF Binding in Mouse ESCs Is Partitioned into Short- and Long-Lived Interactions

(A) TF dynamics model. TFs display 3D diffusion (with diffusion time τ_{diff}) and short- and long-lived DNA binding (with residence times τ_{short} and τ_{long}). Short-lived binding occurs at off-target sites (blue) and facilitates 1D sliding, whereas long-lived binding occurs at specific sites (red).

(B) Oct4-paGFP ACF curves (gray and black) satisfactorily fitted with the model comprising diffusion and two binding components (also shown separately).

(C) Single-cell measurements reveal two distinct TF-DNA-binding fractions with mean residence times of ~10 (blue) and ~200 ms (red). Circles represent single cells, and the box is the mean value.

(D and E) Oct4-paGFP DNA-binding properties following treatment with drugs perturbing DNA accessibility (D), mutation of DNA-binding domains, or manipulations preventing TF interactions with ESET (E).

Data are represented as mean ± SEM; n, number of cells; p values are determined by Student's t test; ***p < 0.001. See also Figure S2 and Table S1.

Here, we first used photo-activatable FCS (paFCS) to determine whether the slower diffusing TFs are binding DNA. For diffusing molecules, the characteristic time for fluctuations increases with the size of the observation volume. By contrast, the characteristic dwell time resulting from TF binding events slower than diffusion is independent of volume size, since it is primarily determined by the unbinding rate (Elson, 2013; Michelman-Ribeiro et al., 2009). We combine paFCS and line scanning (Ruan et al., 2004) to test the effect of volume size on the autocorrelation function (ACF) (Figure 1B). After photo-activating a nuclear fraction of Oct4 molecules fused to paGFP (Oct4-paGFP) in live ESCs, we repeatedly scan along an intranuclear line and calculate the ACF curve at each pixel (ACF_{pixel}). The line sampling frequency of these experiments (~1,000 Hz) permits observation of dynamics within 1–1,000 ms. Alternatively, the intensity along the line can be binned and analyzed as a function of time to obtain an ACF curve for the binned data (ACF_{bin}). While the observation volume in ACF_{pixel} is given by the point spread function, the volume for ACF_{bin} is the convolution of multiple scanned volumes (Figure 1B). Monte Carlo simulations demonstrate a distinct shift between ACF_{pixel} and ACF_{bin} for molecules exhibiting diffusion only, yet in the presence of binding slower than diffusion the ACFs are indistinguishable (Figure 1C). As the same data are used for ACF_{pixel} and ACF_{bin}, differences between curves are not due to sampling different regions. The ACFs obtained in live cells are independent of the observation volume size (Figure 1D), and thus the dynamics observed in the slower time window arise from binding events.

Since the experimental ACF differs from the simulated data, describing the behavior of the TFs may require more than one binding term. Oct4-paGFP dynamics cannot be modeled by considering only diffusion and binding to a uniform population of DNA targets (Kaur et al., 2013). Therefore, we extend a model based on a diffusion-limited reaction (Michelman-Ribeiro et al., 2009) to include two binding populations exhibiting long-lived or short-lived binding interactions (Figure 2A). The ACF can be written as

$$G(\tau) = \frac{1}{2^{3/2}N}\left[f_{diff}\left(1+\frac{\tau}{\tau_{diff}}\right)^{-1}\left(1+\frac{\tau}{\omega^2\tau_{diff}}\right)^{-1/2} + f_{short}e^{-\tau/\tau_{short}} + f_{long}e^{-\tau/\tau_{long}}\right], \quad (1)$$

where N is the mean number of photo-activated TFs, τ_{diff} is the characteristic diffusion time, ω is the ratio between axial and radial waists of the observation volume, and f_{diff} is the freely diffusing fraction. This model describes the TF fractions bound to each type of genomic site (f_{long} and f_{short}) and their characteristic residence times (τ_{long} and τ_{short}), which is the inverse of the unbinding rate constant. Simulations incorporating two populations of binding sites with distinct residence times produced ACF curves adequately fitted with Equation 1 and accurately recover parameters characterizing binding (Figure S1A). Moreover, Oct4-paGFP ACF curves fitted with this model exhibit lower residuals than those fitted with a model with one type of binding site (Figure S1B). About 30% of the TFs are bound to DNA with two different residence times of ~10 and ~200 ms (Figures 2A–2C and S1). These results demonstrate the existence of two distinct modes of TF-DNA interactions, discriminated by the binding duration.

We verified the sensitivity of our approach in detecting changes in binding upon manipulation of DNA accessibility, mutation of the TF's DNA-binding domain, or perturbation of interactions with epigenetic regulators. Promoting DNA accessibility with trichostatin A (TSA) (Yoshida et al., 1995) increases the number of both long- and short-lived DNA interactions (Figure 2D; Table S1). Conversely, actinomycin D (ActD), which binds pre-melted DNA within transcriptional complexes (Paramanathan et al., 2012; Sobell, 1985), decreases only the long-lived bound fraction, suggesting that this fraction represents binding to transcriptionally active sites. A point mutation in the recognition helix of Oct4 that disrupts DNA binding and reduces transcriptional efficiency ($Oct4_{V234P}$-paGFP) (Vigano and Staudt, 1996) decreases only long- and short-lived residence times (Figure 2E). Therefore, treatments that alter DNA accessibility affect the fractions of bound TFs without necessarily impacting their residence times, whereas manipulations proposed to change the affinity of the TF for DNA alter residence times without affecting the bound fraction.

Oct4 promotes pluripotency by binding via its SUMOylation-interacting domain (SIM) to ESET (Yeap et al., 2009; Yuan et al., 2009). Both ESET knockdown and mutation of the Oct4 SIM domain ($Oct4\Delta_{SIM}$-paGFP) reduce the residence times for long- and short-lived binding (Figure 2E). A point mutation inhibiting Oct4 SUMOylation by sumo-1 ($Oct4_{K118R}$paGFP) (Wei et al., 2007) does not affect the DNA-binding parameters (Figure 2E), consistent with normal pluripotent lineage development in *sumo1*-null embryos (Zhang et al., 2008). These results suggest that the bound fraction of a TF can be modulated by changes in DNA accessibility, whereas residence times are more sensitive to structural modifications likely affecting the TF's affinity to DNA.

TFs Display Long- and Short-Lived DNA Interactions in a Lineage-Specific Manner In Vivo

Next, we investigated the DNA-binding dynamics of Oct4-paGFP and Sox2 fused to paGFP (paGFP-Sox2) in live embryos. Immunofluorescence reveals that all cells express Oct4 and Sox2 during early development and their expression is restricted to inner cells by blastocyst stage (Figure S2). paFCS measurements at 16- to 32-cell stage show that for both Oct4-paGFP and paGFP-Sox2, the short-lived bound fraction and residence time are similar between lineages (Figures 3A and 3B; Table S2). However, for the long-lived binding events, inner cells show a larger fraction and longer residence time than outer cells. This suggests that the accessibility of specific sites and the TF's affinity for them may be differentially regulated between lineages. Cdx2, a TF important for extraembryonic cells (Jedrusik et al., 2008; Strumpf et al., 2005), shows a longer residence time in outer cells, suggesting that its function is largely regulated by affinity to its specific sites (Figure S3). Therefore, TFs important for pluripotent and extraembryonic cells display lineage-specific DNA-binding properties.

Four-Cell Blastomeres Show Reduced Oct4-paGFP Binding to DNA but Exhibit Cell-to-Cell Variability in the Long-Lived Bound Fraction of paGFP-Sox2

Since previous work proposed that heterogeneities biasing cell fate might be traceable to the four-cell stage, we determined the DNA-binding properties of Oct4-paGFP and paGFP-Sox2 at this stage (Figure 3C). The total DNA-bound fraction of Oct4-paGFP is smaller in four-cell blastomeres than in inner cells at the 16- to 32-cell stage (Table S2). Conversely, the total bound fraction of paGFP-Sox2 is larger than that of Oct4-paGFP, and moreover, significant cell-to-cell variability exists selectively in the paGFP-Sox2 long-lived bound fraction in the four-cell embryo (Figure 3C; Table S2).

We then determined the cellular origin of paGFP-Sox2 binding variability within the embryo. We co-microinjected RNAs for paGFP-Sox2 and H2B-RFP at the one-cell stage and tracked each cell using time-lapse imaging during the 2- to 4-cell transition (Figure 4A). We performed paFCS in each blastomere at the 2- and 4-cell stage. At the two-cell stage, each blastomere within an embryo exhibits similar binding dynamics for both the long- and short-lived fractions. By contrast, at the four-cell stage, there is a selective increase in the long-lived bound fraction in one cell of each pair of sister blastomeres (Figures 4B and 4C; Table S3). The short-lived bound fraction and residence times are similar between all four-cell blastomeres (Figure 4C). These results suggest that heterogeneities in Sox2-DNA binding arising at the four-cell stage may be related to cell fate.

Carm1-Mediated H3R26 Methylation Regulates the Long-Lived Binding of paGFP-Sox2

The differences in the long-lived bound fraction of paGFP-Sox2 between four-cell blastomeres could result from changes in accessibility of specific DNA sites. Since variations in H3 arginine methylation occur at the four-cell stage (Torres-Padilla et al., 2007), we tested whether this epigenetic modification regulates DNA binding. As the methylation of H3 arginine residues 2, 17, and 26 is mediated by Carm1 and co-varies during early development, we used H3R26me2 levels as a readout (Torres-Padilla et al., 2007). We microinjected RNAs for paGFP-Sox2 and H2B-RFP at the one-cell stage and then microinjected RNAs for a membrane-targeted mCherry and membrane-targeted paGFP

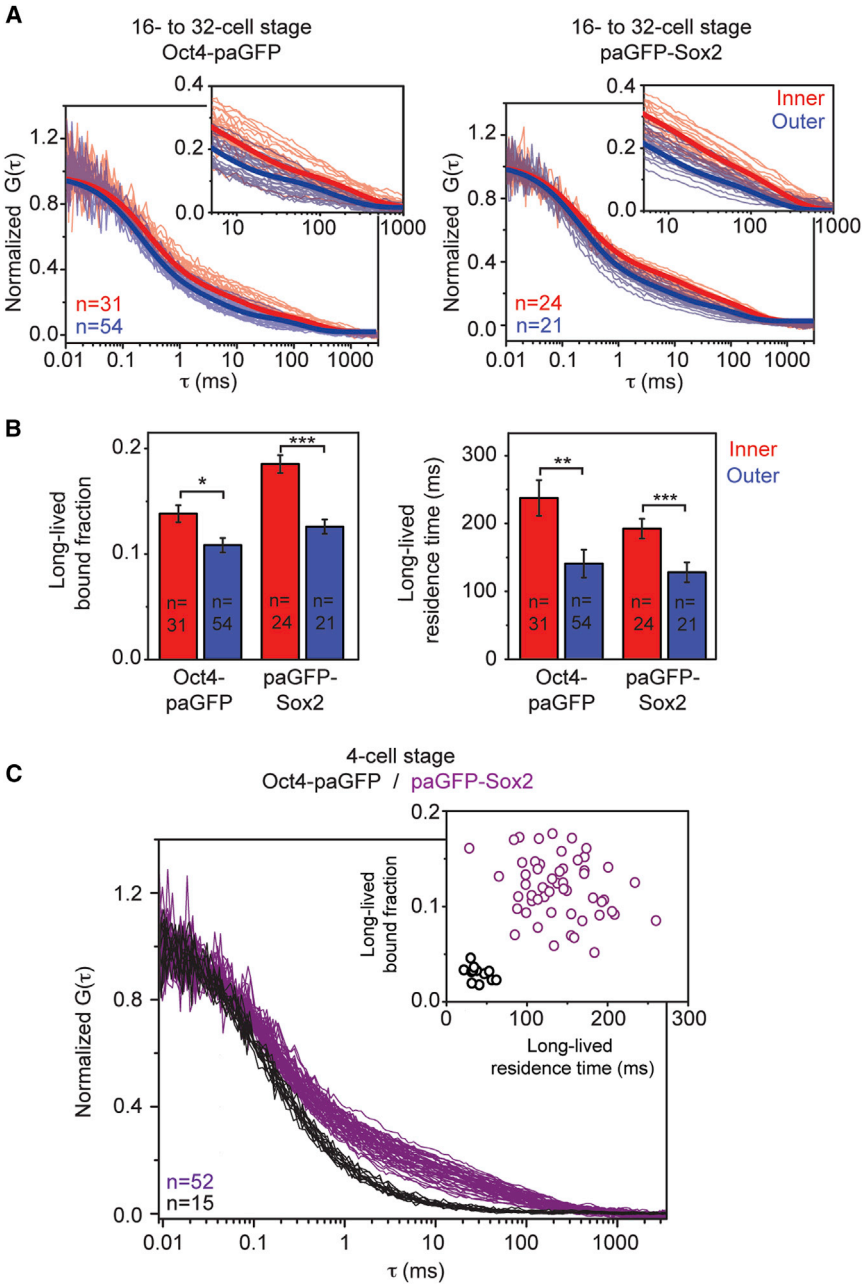

Figure 3. DNA-Binding Properties of Oct4-paGFP and paGFP-Sox2 in the Live Embryo Are Lineage and Developmental Stage Specific

(A) ACFs and mean fits in inner and outer cells. Insets show differences in the time window in which TF-DNA binding takes place.

(B) Oct4-paGFP and paGFP-Sox2 display a larger long-lived bound fraction and a longer residence time in inner compared to outer cells.

(C) Comparison between Oct4-paGFP and paGFP-Sox2 in four-cell embryos. Inset shows single-cell measurements for each TF. While Oct4-paGFP shows consistently reduced binding to DNA, paGFP-Sox2 displays more binding and pronounced cell-to-cell variability.

Data are represented as mean ± SEM; p values are determined by Student's t test; ***p < 0.001, **p < 0.01, *p < 0.05; in (A) and (C) each trace represents an ACF curve obtained from a single cell. See also Figure S3 and Table S2.

in only one cell at the two-cell stage (Figure 5A). Next, we performed paFCS in the memb-mCherry-positive sister cells at the four-cell stage. Using a two-photon laser to selectively photo-activate the membrane, we marked the cell with the larger long-lived bound fraction and then fixed the embryos to measure H3R26me2 levels by immunofluorescence, correcting for light scattering at different z positions. The marked four-cell blastomeres showing the larger long-lived paGFP-Sox2 bound fraction also exhibit higher levels of H3R26me2 than their sister cells (Figure 5A).

In line with previous work (Torres-Padilla et al., 2007), H3R36me2 levels and the long-lived paGFP-Sox2-bound fraction correlate with the orientation of cell cleavages during the 2- to 4-cell stage (Figure S4). In tetrahedral embryos, H3R26me2 levels and the long-lived paGFP-Sox2-bound fraction vary between sister blastomeres. Vegetal blastomeres produced by meridional-equatorial (ME) cleavages show the lowest bound fraction of paGFP-Sox2 and least H3R26 methylation. Moreover, there are no differences in H3R36me2 levels or Sox2-DNA binding between blastomeres in planar embryos. Image segmentation (Samarage et al., 2015) enabled us to also reveal differences in H3R26me2 levels and long-lived paGFP-Sox2 binding between blastomeres produced by equatorial-meridional cleavages, although these were smaller than those in ME embryos.

Next, we explored the origin of different paGFP-Sox2-binding dynamics and H3R26me2 variability. For the two-cell stage analysis, we fixed and immunolabeled the embryos with H3R26me2 or Carm1 antibodies. For the four-cell stage analysis, we microinjected memb-mCherry into one cell of the two-cell embryo to generate pairs of memb-mCherry-positive and memb-mCherry-negative sister cells at the four-cell stage (Figure 5B). Like paGFP-Sox2 long-lived binding, both H3R26me2 and Carm1 levels are initially indistinguishable between two-cell blastomeres. However, they selectively increase in one cell of each pair of sister blastomeres at the four-cell stage. Therefore, differences in paGFP-Sox2 binding arise concurrently with cell-to-cell variability in H3R26me2 and Carm1 levels within the four-cell embryo.

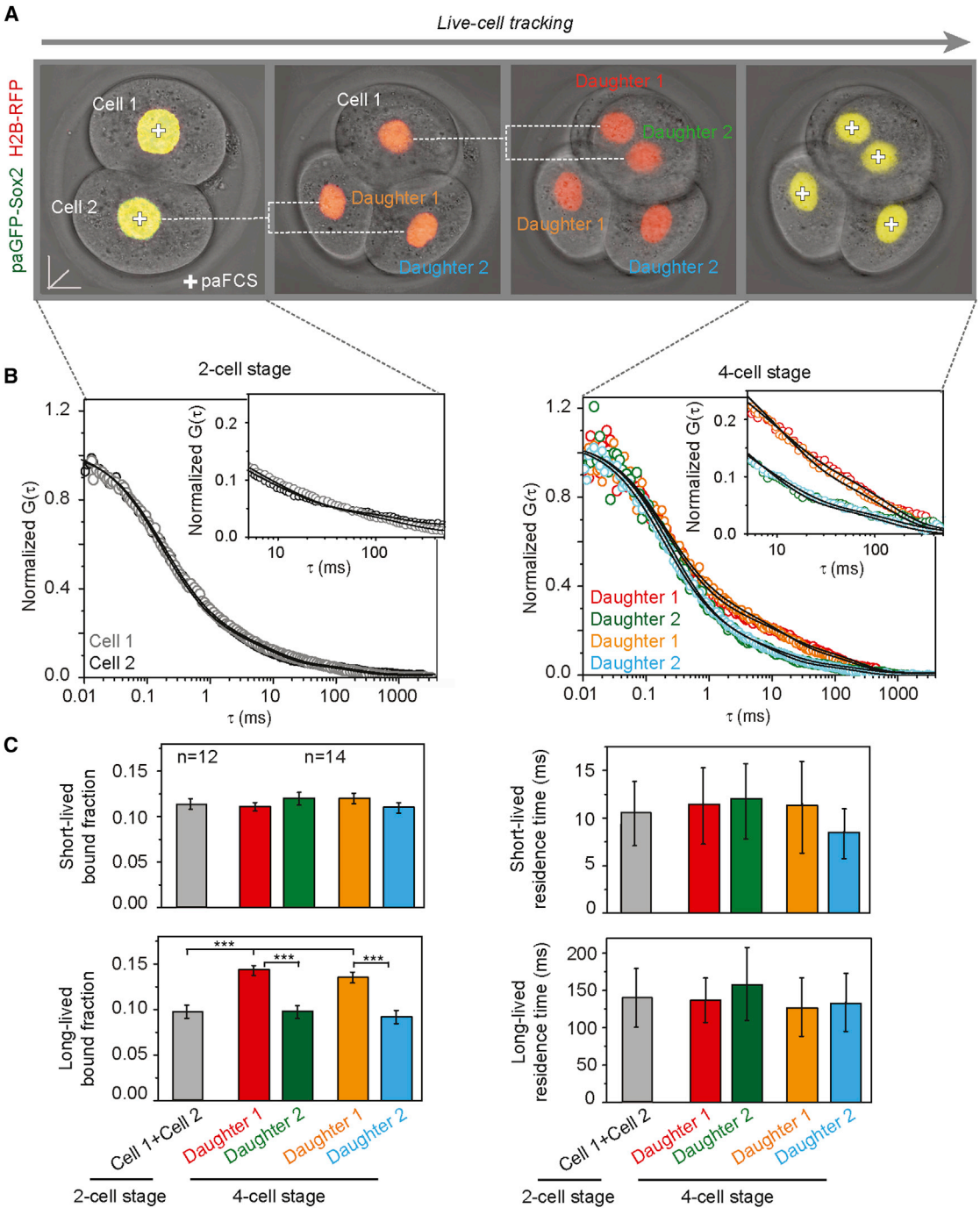

Figure 4. paGFP-Sox2 Exhibits More Long-Lived DNA-Binding Events in Two Cells of the Four-Cell Embryo

(A) Combining cell tracking and paFCS to reveal the DNA-binding properties of paGFP-Sox2 in 2- and 4-cell blastomeres. Snapshots of a live embryo micro-injected at one-cell stage with RNAs for paGFP-Sox2 and H2B-RFP. Dashed lines trace cell lineages. Scale bar, 10 μm in xyz.

(B) paFCS measurements of each blastomere at the 2- and 4-cell stage. Each blastomere at the two-cell stage (left, cell 1 and cell 2) produces two daughter cells with distinct ACF curves (right, circles; black lines show fits). Inset highlights differences between ACF curves in time window associated with DNA binding.

(C) During the 2- to 4-cell stage, the long-lived DNA-bound fraction of paGFP-Sox2 increases selectively in one cell of each pair of sister blastomeres at the four-cell stage. The short-lived bound fraction and residence times are similar among all cells. Each bar represents one cell of the embryo, except for the two-cell stage, where there are no significant differences between cells.

Data are represented as mean ± SEM; p values are determined by Student's t test; ***$p < 0.001$; n, number of embryos. See also Table S3.

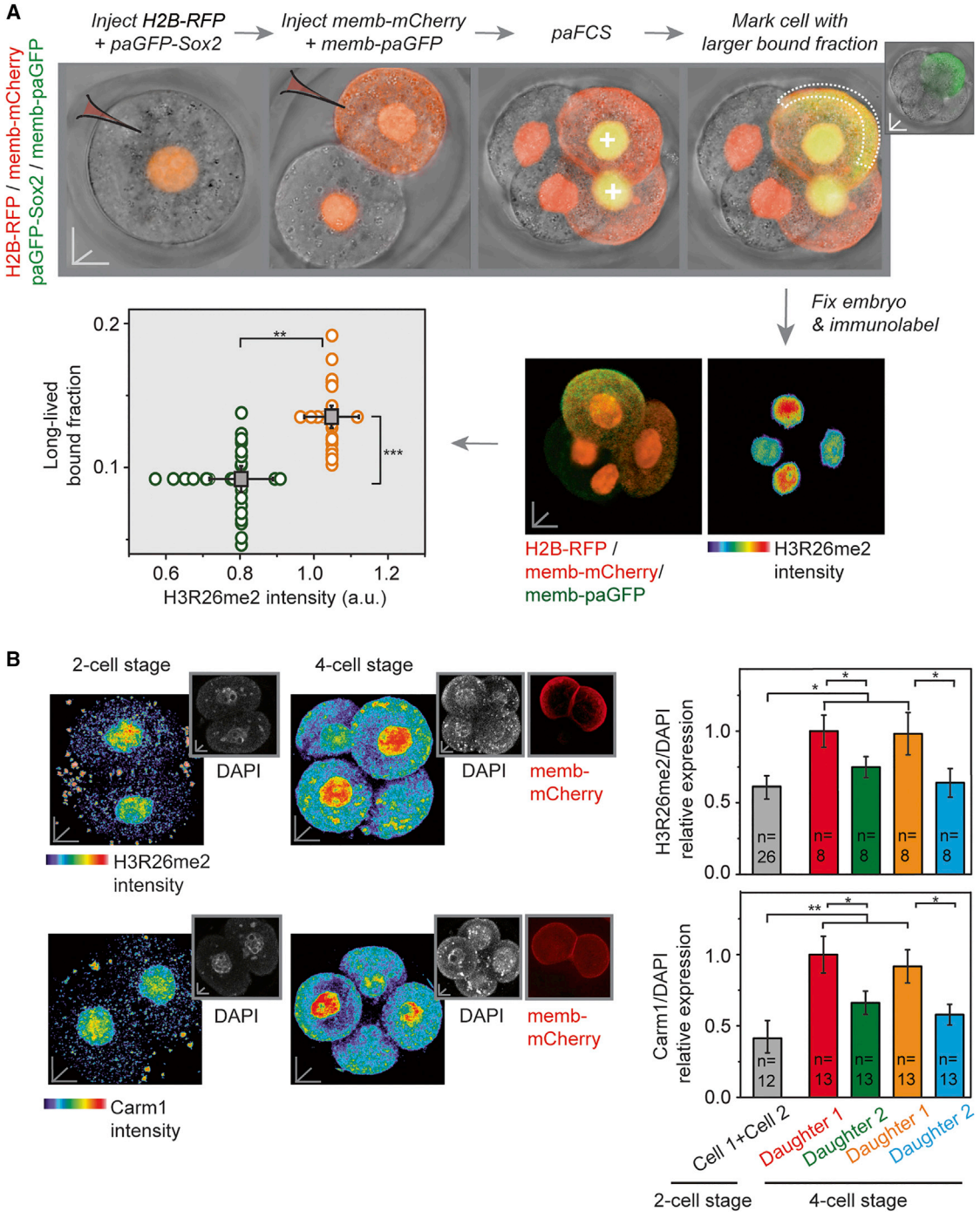

Figure 5. Four-Cell Blastomeres with Larger Long-Lived paGFP-Sox2-Bound Fractions Exhibit Higher H3R26me2 Levels

(A) Correlating paGFP-Sox2-DNA binding and H3R26me2 levels. An embryo is microinjected with RNAs for paGFP-Sox2 and H2B-RFP at the one-cell stage. At the two-cell stage, only one cell is microinjected with RNAs for memb-mCherry and memb-paGFP. At the four-cell stage, paFCS is performed in the pair of memb-mCherry-labeled cells. The cell with the larger long-lived paGFP-Sox2-bound fraction is marked via photo-activation of memb-paGFP (white line). The embryos are then batch processed for H3R26me2 immunolabeling to minimize variability. Individual data points for the long-lived bound fractions of paGFP-Sox2 (vertical) and levels of H3R26me2 (horizontal) are shown on the same graph. Cells with a larger long-lived bound fraction display higher levels of H3R26me2. Each circle represents a single cell along each axis (n = 24 cells from 12 embryos), and the boxes represent mean values.

(B) Correlating H3R26me2 and Carm1 levels in blastomeres of 2- and 4-cell embryos. For the two-cell stage analysis, the embryos were fixed and immunolabeled for H3R26me2 (n = 26 cells from 13 embryos) or Carm1 (n = 12 cells from 6 embryos). To distinguish each pair of sister blastomeres in four-cell embryos, memb-mCherry RNA was microinjected into one cell at the two-cell stage, resulting in memb-mCherry-positive and memb-mCherry-negative daughter cells. H3R26me2

(legend continued on next page)

Carm1 Downregulation Decreases the Long-Lived Bound Fraction of paGFP-Sox2 and Expression of Sox2 Targets

Next, we determined whether manipulation of H3R26me2 levels affects DNA binding. Microinjection of Carm1 small interfering RNAs (siRNAs) into one cell of the two-cell embryo reduced Carm1 mRNA and protein (Figure S5) and H3R26me2 levels (Figure 6A) in the knockdown progeny at the four-cell stage compared to uninjected cells. Carm1 downregulation also reduces the long-lived bound fraction of paGFP-Sox2 (Figure 6B; Table S4). However, there is no change in the short-lived bound fraction or the residence times for both fractions. Although Carm1 can directly methylate Sox2 (Zhao et al., 2011), the DNA-binding properties of a Sox2 mutant unable to be methylated by Carm1 (paGFP-Sox2$_{R113K}$) are indistinguishable from those of paGFP-Sox2 (Figure S6; Table S2). This suggests that Carm1 controls paGFP-Sox2 DNA binding by methylating histones, and not the Sox2 protein. We cannot perform genome-wide chromatin-binding experiments on single cells of the embryo to show how a reduction of the long-lived paGFP-Sox2 bound fraction changes the occupancy of Sox2 targets. Nevertheless, we find that Carm1 downregulation decreases the mRNA and protein expression of Sox2 targets associated with pluripotency, including *Sox2* itself, *Oct4*, and *Nanog* (Figures 6C and 6D). Carm1 knockdown also reduces the mRNA levels of genes expressed in the pre-implantation embryo and proposed to be targets of Sox2, but not of Oct4, including *cacna1a* (Biase et al., 2014), *per2* (Amano et al., 2009), *kcnh8* (Boyer et al., 2005; Maekawa et al., 2007), and *pin2* (Ben-Porath et al., 2008; Boyer et al., 2005; Zeng and Schultz, 2005) (Figure S5B). Although Carm1 downregulation does not affect Oct4-paGFP-DNA binding at the four-cell stage, it reduces its long-lived bound fraction at the eight-cell stage, when this TF first establishes cell-to-cell variability (Figures S6B and S6D). Consistent with models proposing that the long-lived DNA-bound fraction of TFs represents interactions yielding gene transcription, these results suggest that Carm1-mediated H3R26 methylation regulates gene expression by altering the accessibility of specific Sox2 binding sites in vivo.

Most Cells Internalized by the 16-Cell Stage Are Derived from Four-Cell Blastomeres with Larger Long-Lived Bound Fractions of paGFP-Sox2

Next, we combined paFCS with time-lapse imaging and image-segmentation techniques (Samarage et al., 2015) to non-invasively examine whether heterogeneities between blastomeres predict cell fate. We microinjected one blastomere at the two-cell stage with RNAs for paGFP-Sox2, H2B-RFP, and memb-mCherry and performed paFCS in labeled sister cells at the four-cell stage to measure the long-lived paGFP-Sox2-bound fractions. We then followed the development of the embryo by imaging at 20-min intervals and segmented cell membranes and nuclei to track lineage allocation (Figure 7A). As the number of inner cells varies markedly between blastocysts (Morris et al., 2010; Samarage et al., 2015), we analyzed the contribution to the pioneering cells that found the inner mass by the 16-cell stage. We found that those four-cell blastomeres with larger long-lived paGFP-Sox2-bound fractions contribute significantly more of the cells that form the inner mass (Figures 7A and S7). Finally, we determined the effects of Carm1 downregulation on inner cell allocation. Microinjection of Carm1 siRNA into one cell at the two-cell stage causes a reduction in the number of inner cells derived from Carm1 knockdown cells (Figure 7B). These results demonstrate that differences in paGFP-Sox2-DNA binding at the four-cell stage predict, and may be required for, the generation of the inner mass.

DISCUSSION

Lineage Allocation in the Mouse Embryo

By relating Sox2-DNA-binding dynamics to cell fate in live embryos our findings demonstrate that cell fates are biased by molecular heterogeneities between four-cell blastomeres. Previous research supports the view that the first cell fates of the embryo may be predictable. The finding of molecular differences between early blastomeres has been demonstrated at the levels of H3R26 methylation (Torres-Padilla et al., 2007) and, more recently, in gene expression patterns (Shi et al., 2015). However, since the techniques used prevent further embryo development, eventual cell fates could not be confirmed. Lineage tracing in transgenic Rainbow mice showed differing contributions of individual four-cell blastomeres to blastocyst lineages (Tabansky et al., 2013). Moreover, disaggregated four-cell blastomeres are not equally efficient at producing chimeric embryos (Piotrowska-Nitsche et al., 2005). These studies, however, could not directly relate cell fate to molecular heterogeneities between early blastomeres. Finally, differences in Oct4 retention in some cell nuclei were proposed to anticipate inner cell fates (Plachta et al., 2011), yet in that study cells were only tracked between the 8- and 16-cell stages. To directly link molecular differences to cell fate, we non-invasively identified heterogeneities between blastomeres of the same embryo and tracked those cells. Combining paFCS, line scanning, and modeling enabled the discovery of differences in paGFP-Sox2 binding to DNA between blastomeres. Time-lapse imaging and segmentation of the live embryos confirms that blastomeres with more paGFP-Sox2 engaged in long-lived DNA interactions are biased to contribute more inner cells at the 16-cell stage.

In Vivo Partitioning of TFs during Development

Probing how TFs bind to DNA in single cells in vivo has previously been unattainable. Chromatin immunoprecipitation techniques are inapplicable in single cells and cannot distinguish binding in sub-minute timescales, while SMT methods are restricted to cell-culture systems (Chen et al., 2014; Liu et al.,

and Carm1 levels are similar between cells at the two-cell stage. In the four-cell embryo, each pair of sister cells comprises one cell with higher and one cell with lower H3R26me2 (n = 8 cells from eight embryos) and Carm1 (n = 13 cells from 13 embryos) levels. Insets show DAPI staining used to correct for light scattering and memb-mCherry labeling.

Data are represented as mean ± SEM; p values are determined by Student's t test. ***$p < 0.001$, **$p < 0.01$, *$p < 0.05$; scale bars, 10 μm in xyz. See also Figure S4.

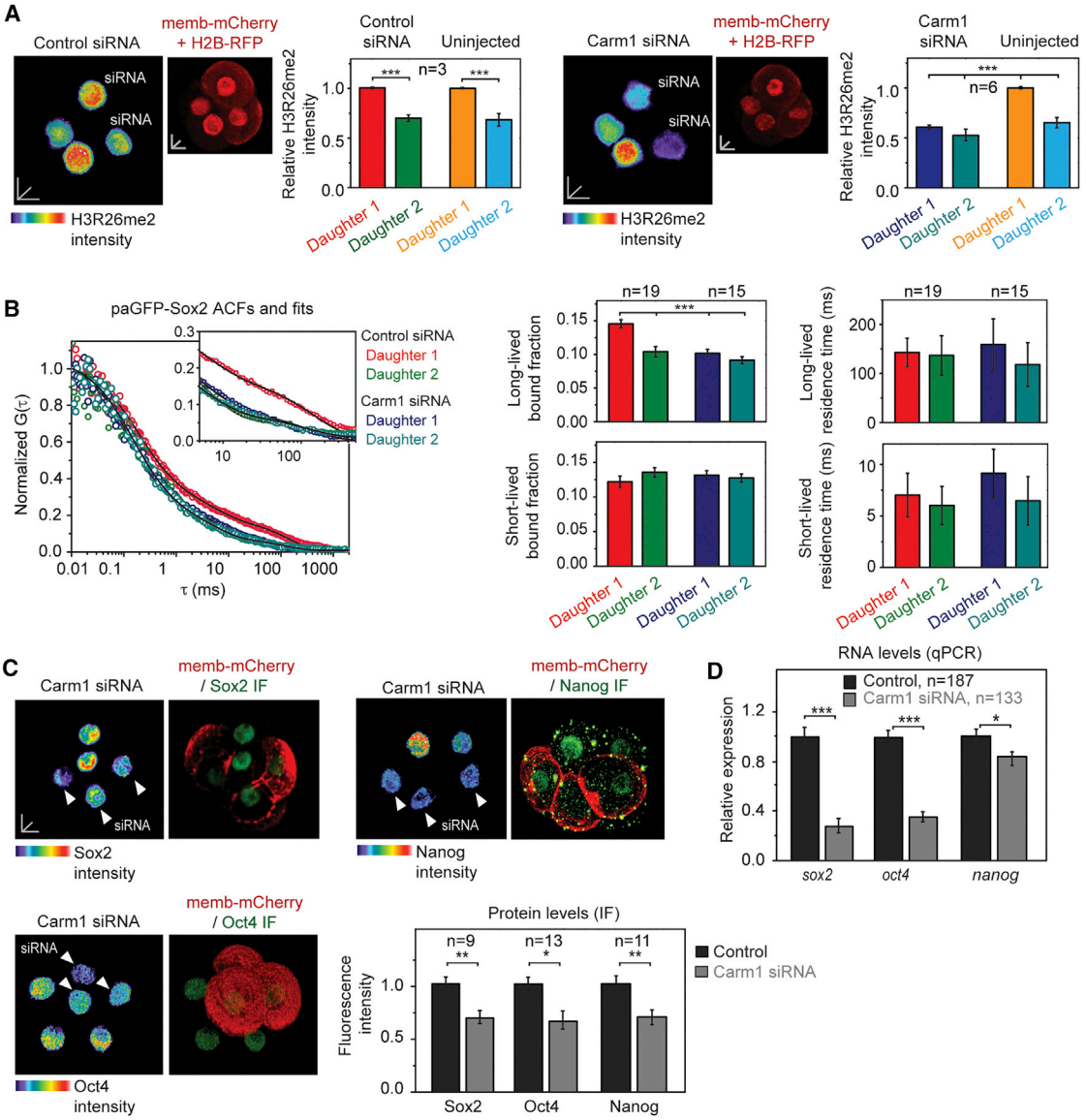

Figure 6. Decreasing H3R26 Methylation Reduces Long-Lived Binding and Expression of Sox2 Targets

(A) H3R26me2 immunolabeling levels in four-cell embryos. At the one-cell stage, embryos were microinjected with H2B-RFP RNA. At the two-cell stage, one cell of the embryo was microinjected with scrambled control or Carm1 siRNAs and memb-mCherry RNA to identify sister cells. H3R26me2 levels were normalized to H2B-RFP to correct for light scattering (n = 3 cells from three embryos). Carm1 downregulation (n = 6 cells from six embryos) decreases H3R26me2 levels.

(B) ACF curves (left) for the daughter cells of a blastomere injected at the two-cell stage with paGFP-Sox2, H2B-RFP, and either Carm1 siRNAs or scrambled siRNA. The pairs of cells with control siRNA give rise to distinct ACF curves (n = 19 cells from 19 embryos). In contrast, the pairs with Carm1 knockdown (n = 14 cells from 14 embryos) show undistinguishable ACF curves and reduced long-lived bound fractions (bar graphs). The short-lived bound fraction and the residence times for both fractions are unaffected by knockdown.

(C) Carm1 downregulation in half of the embryo reduces levels of Sox2, Oct4, and Nanog. At the two-cell stage, one cell was microinjected with memb-mCherry and Carm1 siRNAs, and the embryo was immunolabeled at the 16-cell stage. Arrowheads indicate knockdown cells identifiable by their memb-mCherry expression. IF, immunofluorescence.

(D) Microinjection of Carm1 siRNAs at the one-cell stage leads to reduced expression of *sox2*, *oct4*, and *nanog* mRNAs, as quantified by qPCR in the 16-cell stage embryo homogenates.

Data are represented as mean ± SEM; n denotes number of cells in (A) and (B) and the number of embryos in (C) and (D); p values are determined by Student's t test; ***p < 0.001, **p < 0.01, *p < 0.05; scale bars, 10 μm in xyz. See also Figures S5, S6, and S7 and Table S4.

2014; Morisaki et al., 2014; Normanno et al., 2015). Our study provides evidence for the repartitioning of TFs between specific and non-specific DNA sites in vivo, in line with current biophysical models. We demonstrate in vivo the existence of three kinetically different TF populations. One population represents ~70% of the molecules and undergoes 3D Brownian diffusion.

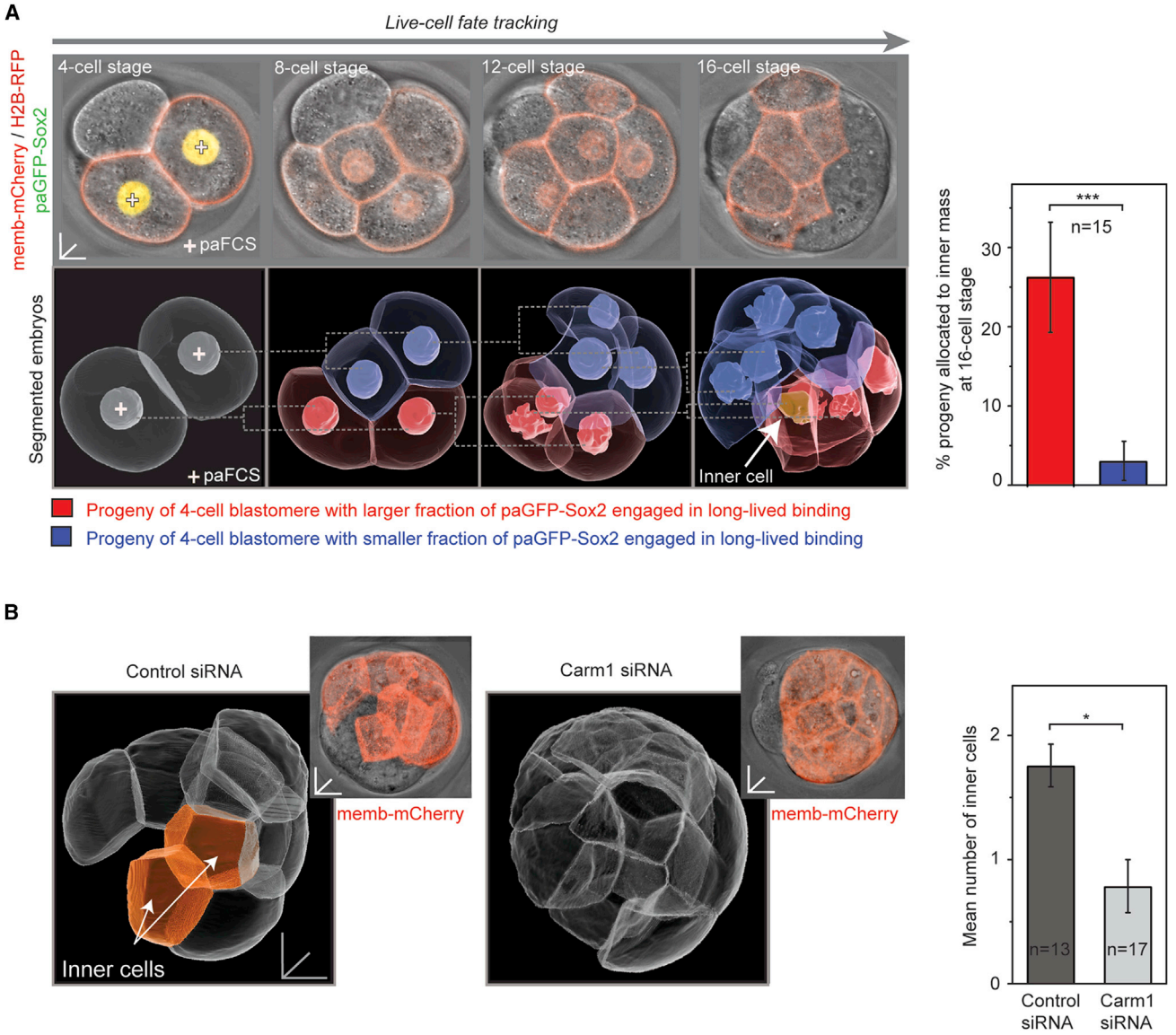

Figure 7. Four-Cell Blastomeres with a Larger Long-Lived Bound Fraction of paGFP-Sox2 Contribute More Inner Cells

(A) Live-cell tracking of the contribution of four-cell blastomeres with distinct long-lived paGFP-Sox2-bound fractions to the inner mass. At the two-cell stage, one cell was microinjected with RNAs for paGFP-Sox2, H2B-RFP, and memb-mCherry. paFCS was performed at the four-cell stage to measure the fraction of paGFP-Sox2 engaged in long-lived DNA interactions. Embryos were then imaged by time-lapse microscopy until the 16-cell stage, and cell nuclei and membranes were computationally segmented to track cell morphology and position. Dashed lines trace cell lineages. Four-cell blastomeres with the larger long-lived bound fraction contribute more inner cells. An inner cell is highlighted in orange.

(B) Carm1 downregulation decreases inner cell numbers. At the two-cell stage, one cell was microinjected with memb-mCherry RNA and Carm1 siRNAs. Images show computationally segmented 16-cell embryos. Fewer inner cells derive from Carm1 siRNA-injected blastomeres.

Data are represented as mean ± SEM; n, number of embryos; p values are determined by Student's t test; ***$p < 0.001$, *$p < 0.05$; scale bars, 10 μm in xyz.

The mean diffusion coefficient approximates that expected for proteins the size of paGFP-Sox2 moving freely in the nucleus (Haustein and Schwille, 2003). The other two populations each account for ~15% of the molecules and are comprised of TFs engaged in DNA binding with residence times of ~10 ms and ~200 ms.

In agreement with current models, our in vivo results indicate that the shorter-lived fraction represents TFs interacting with DNA in a non-specific manner, which could include 1D TF sliding and hopping (Chen et al., 2014; Doucleff and Clore, 2008; Gorman et al., 2010; Hammar et al., 2012; Mueller et al., 2013). Longer-lived binding likely represents specific TF-DNA interactions. The residence times we obtained are consistent with those measured for Oct4 and Sox2 in vitro (Chen et al., 2014), after accounting for the temporal resolution of each experimental approach and the cellular context.

More generally, we confirm the hypothesis that TF-DNA binding dynamics change during cell fate determination in vivo (Biggin, 2011; Hager et al., 2009; Mueller et al., 2013). In lineages in which Sox2 and Oct4 are developmentally required, their DNA-bound fractions are larger and their residence times longer, reflecting more stable interactions. Furthermore, even before the embryo establishes its first distinguishable lineages, Sox2 DNA-binding dynamics differ between four-cell blastomeres. Only a small total fraction of Oct4 is bound to DNA in the four-cell embryo, and this binding is pre-dominantly short lived. Sox2 and Oct4 heterodimerize to drive expression of some gene targets (Boyer et al., 2006; Chen et al., 2008). Although we cannot experimentally dissect heterodimerization dynamics in single cells of live embryos, it is plausible that the initial engagement of Sox2 in long-lived DNA binding may be independent of heterodimerization. Therefore, the stage-specific increase in long-lived DNA binding of paGFP-Sox2 preceding that of Oct4-paGFP in the embryo may represent a physiological correlate of the hierarchical assembly of the pluripotency enhanceosome recently uncovered in embryonic stem cells (ESCs) (Chen et al., 2014).

Epigenetic Regulation of TF-DNA Binding In Vivo

Our findings open two questions: (1) what mechanisms lead to different Sox2-DNA-binding dynamics, and (2) do differences in long-lived binding actually bias cell fate? In agreement with suggestions that H3R26me2 facilitates an open chromatin structure (Burton and Torres-Padilla, 2014; Torres-Padilla et al., 2007), we propose that Sox2-DNA binding is one of the processes that H3R26 methylation controls by regulating the accessibility of TF-specific DNA sites. When H3R26me2 levels are lowered by Carm1 downregulation, only the long-lived bound fraction is affected, without accompanying changes in the short-lived fraction. However, not all long-lived binding is lost, suggesting that Sox2-DNA binding may be independent of H3R26me2 levels at some sites.

The increase in long-lived Sox2-DNA binding resulting from H3R26 methylation might bias fate by modulating transcription. This idea is supported by our findings that H3R26me2 levels correlate with paGFP-Sox2 long-lived binding in the early embryo and that Carm1 downregulation reduces expression of Sox2 targets and inner cell numbers. However, in line with largely normal pre-implantation development of *Sox2*-null embryos (Avilion et al., 2003; Wicklow et al., 2014), it is plausible that embryonic plasticity combined with compensatory mechanisms observed in knockout models (Rossi et al., 2015), can still overwhelm the effects of Sox2 deficiency.

Conclusions

We show that TFs undergo temporally distinct binding events with DNA in the living mouse embryo. Developmentally regulated epigenetic changes create differences in the fraction of paGFP-Sox2 engaged in long-lived DNA binding between four-cell blastomeres, which predict a bias in the allocation of the first inner cells of the embryo. The variability between four-cell blastomeres may originate from the interplay between cell cleavage orientations (Zernicka-Goetz et al., 2009), differences in gene expression (Shi et al., 2015) triggered by noise-excitable mechanisms (Eldar and Elowitz, 2010) and the uneven distribution of yet unidentified factors.

EXPERIMENTAL PROCEDURES

Mouse work was carried out following animal ethics guidelines of the Agency for Science, Technology and Research (Singapore).

Mouse Embryo and ESC Work

RNA production, embryo microinjection, and ESC work were performed as described (Kaur et al., 2013). RNAs were microinjected at 120 ng μl^{-1} (Oct4-paGFP, paGFP-Sox2, and Cdx2-paGFP), 25 ng μl^{-1} (H2B-RFP), and 40 ng μl^{-1} (memb-mCherry, memb-paGFP). For blastocyst experiments, DNA was microinjected as described (Kaur et al., 2013). Carm1 siRNAs (mPrmt4-siRNA-A sense 5′ ACCAAAUCAAGUCCAGGCCCGTT-3′ and mPrmt4-siRNA-B 5′- UCACAGCCCUCUUUGCUAUGGTT-3′, Silencer Select, ThermoFisher) or scrambled control (Stealth RNAi Negative control Lo GC, ThermoFisher) were microinjected at 200 nM. Total mRNA was extracted using an Arcturus PicoPureAR Kit (Applied Biosystems) and RNase-Free DNase Set (QIAGEN). qRT-PCR was performed using a TaqManAR RNA-to-CT 1-Step Kit (Applied Biosystems) and Lightcycler 480II qPCR (Roche). TaqMan Gene Expression Assays (Applied Biosystems) were used to determine expression for *carm1* (Mm00491417_m1), *pou5f1* (Mm03053917_g1), *sox2* (Mm03053810_s1), *nanog* (Mm02019550_s1), *cacna1a* (Mm00432190_m1), *per2* (Mm00478099_m1), *kcnh8* (Mm01277239_m1), *pin2* (Mm00436928_m1), and *18S* (Mm03928990_g1). ESET siRNAs were used as described (Kaur et al., 2013). Cell tracking and segmentation have been described previously (Samarage et al., 2015). Immunofluorescence was performed as described (Kaur et al., 2013; Samarage et al., 2015) with antibodies for Carm1, 1:150 (3379, Cell Signaling Technology), H3R26me2, 1:150 (127095, Abcam), Sox2, 1:200 (59776, Abcam), Oct4, 1:400 (8628, Santa Cruz), Nanog 1:200 (80892, Abcam), and Cdx2 1:200 (88129, Abcam). Protein levels were measured on maximum fluorescence intensity projections of nuclei normalized against H2B-RFP or DAPI.

Imaging and paFCS

We used a Zeiss LSM780 confocal microscope and water Apochromat 40X 1.2 na objective. Photo-activation and paFCS were performed as previously described (Kaur et al., 2013). Fluorescence intensity was recorded in 200-ns bins for 10 to 20 s and 7 to 10 repetitions. ACF curves were fitted with Equation 1 applying a global routine to each dataset and assuming common k_{off} values. This enables recovery of decay constants when fitting multiple exponential functions (Beechem, 1992). Equation 1 neglects GFP photo-physics observed at short time lags to minimize the number of fitting parameters (Wachsmuth et al., 2000). For line scanning, fluorescence was detected with gallium arsenide phosphite photo-multiplier detectors along a 2- to 3-μm line for 200 s at 1,000 Hz.

Statistical Analysis

Analyses were performed with GraphPad Prism and Matlab. An unpaired, two-tailed Student's t test was used, with the assumption of unequal variances. Reproducibility was confirmed by independent experiments.

SUPPLEMENTAL INFORMATION

Supplemental Information includes Supplemental Experimental Procedures, seven figures, and five tables and can be found with this article online at http://dx.doi.org/10.1016/j.cell.2016.02.032.

A video abstract is available at http://dx.doi.org/10.1016/j.cell.2016.02.032#mmc3

AUTHOR CONTRIBUTIONS

M.D.W., Y.D.A., G.K., Z.W.Z., and S.B. performed the experiments. J.F.A., V.L., Y.D.A., E.M., and L.B. performed modeling and FCS analysis. M.D.W., J.F.A., Y.D.A., Z.W.Z., S.B., V.L., and N.P. wrote the paper.

ACKNOWLEDGMENTS

We thank Juan Silva for embryo microinjections. This work was supported by A*STAR Investigatorship and EMBO Young Investigator grants (to N.P.) and ANPCyT (PICT 2012-0899) and UBACyT (20020110100074) grants (to V.L.); E.M., L.B., and V.L. are CONICET members. Z.W.Z. is supported by an A*STAR National Science Scholarship.

Received: November 30, 2015
Revised: January 20, 2016
Accepted: February 11, 2016
Published: March 24, 2016

REFERENCES

Amano, T., Matsushita, A., Hatanaka, Y., Watanabe, T., Oishi, K., Ishida, N., Anzai, M., Mitani, T., Kato, H., Kishigami, S., et al. (2009). Expression and functional analyses of circadian genes in mouse oocytes and preimplantation embryos: Cry1 is involved in the meiotic process independently of circadian clock regulation. Biol. Reprod. *80*, 473–483.

Ashall, L., Horton, C.A., Nelson, D.E., Paszek, P., Harper, C.V., Sillitoe, K., Ryan, S., Spiller, D.G., Unitt, J.F., Broomhead, D.S., et al. (2009). Pulsatile stimulation determines timing and specificity of NF-kappaB-dependent transcription. Science *324*, 242–246.

Avilion, A.A., Nicolis, S.K., Pevny, L.H., Perez, L., Vivian, N., and Lovell-Badge, R. (2003). Multipotent cell lineages in early mouse development depend on SOX2 function. Genes Dev. *17*, 126–140.

Beechem, J.M. (1992). Global analysis of biochemical and biophysical data. Methods Enzymol. *210*, 37–54.

Ben-Porath, I., Thomson, M.W., Carey, V.J., Ge, R., Bell, G.W., Regev, A., and Weinberg, R.A. (2008). An embryonic stem cell-like gene expression signature in poorly differentiated aggressive human tumors. Nat. Genet. *40*, 499–507.

Ben-Tabou de-Leon, S., and Davidson, E.H. (2007). Gene regulation: gene control network in development. Annu. Rev. Biophys. Biomol. Struct. *36*, 191.

Biase, F.H., Cao, X., and Zhong, S. (2014). Cell fate inclination within 2-cell and 4-cell mouse embryos revealed by single-cell RNA sequencing. Genome Res. *24*, 1787–1796.

Biggin, M.D. (2011). Animal transcription networks as highly connected, quantitative continua. Dev. Cell *21*, 611–626.

Boyer, L.A., Lee, T.I., Cole, M.F., Johnstone, S.E., Levine, S.S., Zucker, J.P., Guenther, M.G., Kumar, R.M., Murray, H.L., Jenner, R.G., et al. (2005). Core transcriptional regulatory circuitry in human embryonic stem cells. Cell *122*, 947–956.

Boyer, L.A., Mathur, D., and Jaenisch, R. (2006). Molecular control of pluripotency. Curr. Opin. Genet. Dev. *16*, 455–462.

Burton, A., and Torres-Padilla, M.E. (2014). Chromatin dynamics in the regulation of cell fate allocation during early embryogenesis. Nat. Rev. Mol. Cell Biol. *15*, 723–734.

Cai, L., Dalal, C.K., and Elowitz, M.B. (2008). Frequency-modulated nuclear localization bursts coordinate gene regulation. Nature *455*, 485–490.

Chen, X., Xu, H., Yuan, P., Fang, F., Huss, M., Vega, V.B., Wong, E., Orlov, Y.L., Zhang, W., Jiang, J., et al. (2008). Integration of external signaling pathways with the core transcriptional network in embryonic stem cells. Cell *133*, 1106–1117.

Chen, J., Zhang, Z., Li, L., Chen, B.C., Revyakin, A., Hajj, B., Legant, W., Dahan, M., Lionnet, T., Betzig, E., et al. (2014). Single-molecule dynamics of enhanceosome assembly in embryonic stem cells. Cell *156*, 1274–1285.

Cohen-Saidon, C., Cohen, A.A., Sigal, A., Liron, Y., and Alon, U. (2009). Dynamics and variability of ERK2 response to EGF in individual living cells. Mol. Cell *36*, 885–893.

Dietrich, J.E., and Hiiragi, T. (2007). Stochastic patterning in the mouse pre-implantation embryo. Development *134*, 4219–4231.

Digman, M.A., and Gratton, E. (2011). Lessons in fluctuation correlation spectroscopy. Annu. Rev. Phys. Chem. *62*, 645–668.

Doucleff, M., and Clore, G.M. (2008). Global jumping and domain-specific intersegment transfer between DNA cognate sites of the multidomain transcription factor Oct-1. Proc. Natl. Acad. Sci. USA *105*, 13871–13876.

Eldar, A., and Elowitz, M.B. (2010). Functional roles for noise in genetic circuits. Nature *467*, 167–173.

Elson, E.L. (2013). Brief introduction to fluorescence correlation spectroscopy. Methods Enzymol. *518*, 11–41.

Gardner, R.L. (2001). Specification of embryonic axes begins before cleavage in normal mouse development. Development *128*, 839–847.

Gebhardt, J.C., Suter, D.M., Roy, R., Zhao, Z.W., Chapman, A.R., Basu, S., Maniatis, T., and Xie, X.S. (2013). Single-molecule imaging of transcription factor binding to DNA in live mammalian cells. Nat. Methods *10*, 421–426.

Gorman, J., and Greene, E.C. (2008). Visualizing one-dimensional diffusion of proteins along DNA. Nat. Struct. Mol. Biol. *15*, 768–774.

Gorman, J., Plys, A.J., Visnapuu, M.L., Alani, E., and Greene, E.C. (2010). Visualizing one-dimensional diffusion of eukaryotic DNA repair factors along a chromatin lattice. Nat. Struct. Mol. Biol. *17*, 932–938.

Hager, G.L., McNally, J.G., and Misteli, T. (2009). Transcription dynamics. Mol. Cell *35*, 741–753.

Halford, S.E., and Marko, J.F. (2004). How do site-specific DNA-binding proteins find their targets? Nucleic Acids Res. *32*, 3040–3052.

Hammar, P., Leroy, P., Mahmutovic, A., Marklund, E.G., Berg, O.G., and Elf, J. (2012). The lac repressor displays facilitated diffusion in living cells. Science *336*, 1595–1598.

Haustein, E., and Schwille, P. (2003). Ultrasensitive investigations of biological systems by fluorescence correlation spectroscopy. Methods *29*, 153–166.

Jedrusik, A., Parfitt, D.E., Guo, G., Skamagki, M., Grabarek, J.B., Johnson, M.H., Robson, P., and Zernicka-Goetz, M. (2008). Role of Cdx2 and cell polarity in cell allocation and specification of trophectoderm and inner cell mass in the mouse embryo. Genes Dev. *22*, 2692–2706.

Kaur, G., Costa, M.W., Nefzger, C.M., Silva, J., Fierro-González, J.C., Polo, J.M., Bell, T.D., and Plachta, N. (2013). Probing transcription factor diffusion dynamics in the living mammalian embryo with photoactivatable fluorescence correlation spectroscopy. Nat. Commun. *4*, 1637.

Kurotaki, Y., Hatta, K., Nakao, K., Nabeshima, Y., and Fujimori, T. (2007). Blastocyst axis is specified independently of early cell lineage but aligns with the ZP shape. Science *316*, 719–723.

Liu, Z., Legant, W.R., Chen, B.C., Li, L., Grimm, J.B., Lavis, L.D., Betzig, E., and Tjian, R. (2014). 3D imaging of Sox2 enhancer clusters in embryonic stem cells. eLife *3*, e04236.

Louvet-Vallée, S., Vinot, S., and Maro, B. (2005). Mitotic spindles and cleavage planes are oriented randomly in the two-cell mouse embryo. Curr. Biol. *15*, 464–469.

Maekawa, M., Yamamoto, T., Kohno, M., Takeichi, M., and Nishida, E. (2007). Requirement for ERK MAP kinase in mouse preimplantation development. Development *134*, 2751–2759.

Michelman-Ribeiro, A., Mazza, D., Rosales, T., Stasevich, T.J., Boukari, H., Rishi, V., Vinson, C., Knutson, J.R., and McNally, J.G. (2009). Direct measurement of association and dissociation rates of DNA binding in live cells by fluorescence correlation spectroscopy. Biophys. J. *97*, 337–346.

Morisaki, T., Müller, W.G., Golob, N., Mazza, D., and McNally, J.G. (2014). Single-molecule analysis of transcription factor binding at transcription sites in live cells. Nat. Commun. *5*, 4456.

Morris, S.A., Teo, R.T., Li, H., Robson, P., Glover, D.M., and Zernicka-Goetz, M. (2010). Origin and formation of the first two distinct cell types of the inner cell mass in the mouse embryo. Proc. Natl. Acad. Sci. USA *107*, 6364–6369.

Motosugi, N., Bauer, T., Polanski, Z., Solter, D., and Hiiragi, T. (2005). Polarity of the mouse embryo is established at blastocyst and is not prepatterned. Genes Dev. *19*, 1081–1092.

Mueller, F., Stasevich, T.J., Mazza, D., and McNally, J.G. (2013). Quantifying transcription factor kinetics: at work or at play? Crit. Rev. Biochem. Mol. Biol. *48*, 492–514.

Nichols, J., Zevnik, B., Anastassiadis, K., Niwa, H., Klewe-Nebenius, D., Chambers, I., Schöler, H., and Smith, A. (1998). Formation of pluripotent stem cells in the mammalian embryo depends on the POU transcription factor Oct4. Cell *95*, 379–391.

Normanno, D., Dahan, M., and Darzacq, X. (2012). Intra-nuclear mobility and target search mechanisms of transcription factors: a single-molecule perspective on gene expression. Biochim. Biophys. Acta *1819*, 482–493.

Normanno, D., Boudarène, L., Dugast-Darzacq, C., Chen, J., Richter, C., Proux, F., Bénichou, O., Voituriez, R., Darzacq, X., and Dahan, M. (2015). Probing the target search of DNA-binding proteins in mammalian cells using TetR as model searcher. Nat. Commun. *6*, 7357.

Paramanathan, T., Vladescu, I., McCauley, M.J., Rouzina, I., and Williams, M.C. (2012). Force spectroscopy reveals the DNA structural dynamics that govern the slow binding of Actinomycin D. Nucleic Acids Res. *40*, 4925–4932.

Perlmann, T., Eriksson, P., and Wrange, O. (1990). Quantitative analysis of the glucocorticoid receptor-DNA interaction at the mouse mammary tumor virus glucocorticoid response element. J. Biol. Chem. *265*, 17222–17229.

Piotrowska-Nitsche, K., Perea-Gomez, A., Haraguchi, S., and Zernicka-Goetz, M. (2005). Four-cell stage mouse blastomeres have different developmental properties. Development *132*, 479–490.

Plachta, N., Bollenbach, T., Pease, S., Fraser, S.E., and Pantazis, P. (2011). Oct4 kinetics predict cell lineage patterning in the early mammalian embryo. Nat. Cell Biol. *13*, 117–123.

Purvis, J.E., Karhohs, K.W., Mock, C., Batchelor, E., Loewer, A., and Lahav, G. (2012). p53 dynamics control cell fate. Science *336*, 1440–1444.

Rosner, M.H., Vigano, M.A., Ozato, K., Timmons, P.M., Poirier, F., Rigby, P.W., and Staudt, L.M. (1990). A POU-domain transcription factor in early stem cells and germ cells of the mammalian embryo. Nature *345*, 686–692.

Rossant, J. (1976). Postimplantation development of blastomeres isolated from 4- and 8-cell mouse eggs. J. Embryol. Exp. Morphol. *36*, 283–290.

Rossant, J., and Tam, P.P. (2009). Blastocyst lineage formation, early embryonic asymmetries and axis patterning in the mouse. Development *136*, 701–713.

Rossi, A., Kontarakis, Z., Gerri, C., Nolte, H., Hölper, S., Krüger, M., and Stainier, D.Y. (2015). Genetic compensation induced by deleterious mutations but not gene knockdowns. Nature *524*, 230–233.

Ruan, Q., Cheng, M.A., Levi, M., Gratton, E., and Mantulin, W.W. (2004). Spatial-temporal studies of membrane dynamics: scanning fluorescence correlation spectroscopy (SFCS). Biophys. J. *87*, 1260–1267.

Samarage, C.R., White, M.D., Álvarez, Y.D., Fierro-González, J.C., Henon, Y., Jesudason, E.C., Bissiere, S., Fouras, A., and Plachta, N. (2015). Cortical Tension Allocates the First Inner Cells of the Mammalian Embryo. Dev. Cell *34*, 435–447.

Schöler, H.R., Dressler, G.R., Balling, R., Rohdewohld, H., and Gruss, P. (1990). Oct-4: a germline-specific transcription factor mapping to the mouse t-complex. EMBO J. *9*, 2185–2195.

Shi, J., Chen, Q., Li, X., Zheng, X., Zhang, Y., Qiao, J., Tang, F., Tao, Y., Zhou, Q., and Duan, E. (2015). Dynamic transcriptional symmetry-breaking in pre-implantation mammalian embryo development revealed by single-cell RNA-seq. Development *142*, 3468–3477.

Sobell, H.M. (1985). Actinomycin and DNA transcription. Proc. Natl. Acad. Sci. USA *82*, 5328–5331.

Strumpf, D., Mao, C.A., Yamanaka, Y., Ralston, A., Chawengsaksophak, K., Beck, F., and Rossant, J. (2005). Cdx2 is required for correct cell fate specification and differentiation of trophectoderm in the mouse blastocyst. Development *132*, 2093–2102.

Tabansky, I., Lenarcic, A., Draft, R.W., Loulier, K., Keskin, D.B., Rosains, J., Rivera-Feliciano, J., Lichtman, J.W., Livet, J., Stern, J.N., et al. (2013). Developmental bias in cleavage-stage mouse blastomeres. Curr. Biol. *23*, 21–31.

Tarkowski, A.K., and Wróblewska, J. (1967). Development of blastomeres of mouse eggs isolated at the 4- and 8-cell stage. J. Embryol. Exp. Morphol. *18*, 155–180.

Torres-Padilla, M.E., Parfitt, D.E., Kouzarides, T., and Zernicka-Goetz, M. (2007). Histone arginine methylation regulates pluripotency in the early mouse embryo. Nature *445*, 214–218.

Vigano, M.A., and Staudt, L.M. (1996). Transcriptional activation by Oct-3: evidence for a specific role of the POU-specific domain in mediating functional interaction with Oct-1. Nucleic Acids Res. *24*, 2112–2118.

von Hippel, P.H., and Berg, O.G. (1989). Facilitated target location in biological systems. J. Biol. Chem. *264*, 675–678.

Wachsmuth, M., Waldeck, W., and Langowski, J. (2000). Anomalous diffusion of fluorescent probes inside living cell nuclei investigated by spatially-resolved fluorescence correlation spectroscopy. J. Mol. Biol. *298*, 677–689.

Wei, F., Schöler, H.R., and Atchison, M.L. (2007). Sumoylation of Oct4 enhances its stability, DNA binding, and transactivation. J. Biol. Chem. *282*, 21551–21560.

Wicklow, E., Blij, S., Frum, T., Hirate, Y., Lang, R.A., Sasaki, H., and Ralston, A. (2014). HIPPO pathway members restrict SOX2 to the inner cell mass where it promotes ICM fates in the mouse blastocyst. PLoS Genet. *10*, e1004618.

Yeap, L.S., Hayashi, K., and Surani, M.A. (2009). ERG-associated protein with SET domain (ESET)-Oct4 interaction regulates pluripotency and represses the trophectoderm lineage. Epigenetics Chromatin *2*, 12.

Yoshida, M., Horinouchi, S., and Beppu, T. (1995). Trichostatin A and trapoxin: novel chemical probes for the role of histone acetylation in chromatin structure and function. BioEssays *17*, 423–430.

Yuan, P., Han, J., Guo, G., Orlov, Y.L., Huss, M., Loh, Y.H., Yaw, L.P., Robson, P., Lim, B., and Ng, H.H. (2009). Eset partners with Oct4 to restrict extraembryonic trophoblast lineage potential in embryonic stem cells. Genes Dev. *23*, 2507–2520.

Zeng, F., and Schultz, R.M. (2005). RNA transcript profiling during zygotic gene activation in the preimplantation mouse embryo. Dev. Biol. *283*, 40–57.

Zernicka-Goetz, M., Morris, S.A., and Bruce, A.W. (2009). Making a firm decision: multifaceted regulation of cell fate in the early mouse embryo. Nat. Rev. Genet. *10*, 467–477.

Zhang, F.P., Mikkonen, L., Toppari, J., Palvimo, J.J., Thesleff, I., and Jänne, O.A. (2008). Sumo-1 function is dispensable in normal mouse development. Mol. Cell. Biol. *28*, 5381–5390.

Zhao, H.Y., Zhang, Y.J., Dai, H., Zhang, Y., and Shen, Y.F. (2011). CARM1 mediates modulation of Sox2. PLoS ONE *6*, e27026.